Shadows of Bonnor black dihole by chaotic lensing

Mingzhi Wang,[1] Songbai Chen,[1,2,3,*] and Jiliang Jing[1,2,3,†]

[1]*Institute of Physics and Department of Physics, Hunan Normal University, Changsha, Hunan 410081, People's Republic of China*

[2]*Key Laboratory of Low Dimensional Quantum Structures and Quantum Control of Ministry of Education, Hunan Normal University, Changsha, Hunan 410081, People's Republic of China*

[3]*Synergetic Innovation Center for Quantum Effects and Applications, Hunan Normal University, Changsha, Hunan 410081, People's Republic of China*

(Received 28 October 2017; published 26 March 2018)

We numerically study the shadows of a Bonnor black dihole through the technique of backward ray tracing. The presence of a magnetic dipole yields nonintegrable photon motion, which sharply affects the shadow of the compact object. Our results show that there exists a critical value for the shadow. When the magnetic dipole parameter is less than the critical value the shadow is a black disk, but when the magnetic dipole parameter is larger than the critical value the shadow becomes a concave disk with eyebrows possessing a self-similar fractal structure. These behaviors are very similar to those of the equal-mass and nonspinning Majumdar-Papapetrou binary black holes. However, we find that the two larger shadows and the smaller eyebrow-like shadows are joined together by the middle black zone for the Bonnor black dihole, which is different from that in the Majumdar-Papapetrou binary black hole spacetime where they are disconnected. With the increase of the magnetic dipole parameter, the middle black zone connecting the main shadows and the eyebrow-like shadows becomes narrow. Our results show that the spacetime properties arising from the magnetic dipole yield interesting patterns for the shadow cast by a Bonnor black dihole.

DOI: 10.1103/PhysRevD.97.064029

I. INTRODUCTION

A shadow is a two-dimensional dark region in the observer's sky corresponding to light rays that fall into an event horizon when propagated backwards in time. It has been shown that the shape and size of the shadow carry the characteristic information of the geometry around the celestial body [1–3], which means that the shadow can be regarded as a useful tool to probe the nature of the celestial body and to further check various theories of gravity. Past investigations [2,3] have indicated that the shadow is a perfect disk for a Schwarzschild black hole and it changes into an elongated silhouette for a rotating black hole due to its dragging effect. The cusp silhouette of a shadow is found in the spacetime of a Kerr black hole with Proca hair [4] and of a Konoplya-Zhidenko rotating non-Kerr black hole [5] when the black hole parameters lie in a certain range. Moreover, the shadow of a black hole with other characteristic parameters has been studied recently [6–22] (for details, see the review [23]), which indicates that these parameters give rise to richer silhouettes for the shadows cast by black holes.

However, most of the above investigations focused only on the cases where the null geodesics are variable separable and the corresponding dynamical systems are integrable. When the dynamical systems are nonintegrable, the motion of photons could be chaotic, which could lead to some novel features for the black hole shadow. Recently, it was shown that due to such chaotic lensing multi-disconnected shadows with fractal structures emerge for a Kerr black hole with scalar hair [24–27] or a binary black hole system [28,29]. Further analysis has shown that these novel patterns with fractal structures in shadows are determined by the nonplanar bound orbits [4] and the invariant phase-space structures [30] of photon motion in the black hole spacetimes. A similar analysis has also been done for cases with ultracompact objects [31,32].

It is well known that there exist enormous magnetic fields around large astrophysical black holes, especially in the nuclei of galaxies [33–36]. These strong magnetic fields could be induced by currents in accretion disks near the supermassive galactic black holes. On the basis of these strong magnetic fields, there are many theoretical models that account for black hole jets, which are one of the most spectacular astronomical events in the sky [37–39]. In general relativity, one of the most important solutions with magnetic fields is the Ernst solution [40], which describes

*Corresponding author.
csb3752@hunnu.edu.cn
†jljing@hunnu.edu.cn

the gravity of a black hole immersed in an external magnetic field. Interestingly, for an Ernst black hole, the polar circumference of the event horizon increases with the magnetic field, while the equatorial circumference decreases. Bonnor's metric [41] is another important solution of the Einstein field equations in vacuum, which describes a static massive object with a dipole magnetic field in which two static extremal magnetic black holes with charges of opposite signs are situated symmetrically on the symmetry axis. For the Bonnor black dihole spacetime, the area of the horizon is finite, but the proper circumference of the horizon surface is zero. In particular, it is not a member of the Weyl electromagnetic class and it cannot be reduced to the Schwarzschild spacetime in the limit without a magnetic dipole. The new properties of spacetime structure originating from magnetic dipoles will lead to chaos in the motion of particles [42–44]. Since the shadow of black hole is determined by the propagation of light rays in the spacetime, it is expected that the chaotic lensing caused by the new spacetime structure will give rise to new effects in the black hole shadow. Therefore, in this paper we focus on studying the shadow of a Bonnor black dihole [41] and probe the effect of the magnetic dipole parameter on the black hole shadow.

The paper is organized as follows. In Sec. II, we briefly review the metric of a Bonnor black dihole and then analyze the propagation of light rays in this background. In Sec. III, we investigate the shadows cast by a Bonnor black dihole. In Sec. IV, we discuss the invariant phase-space structures of photon motion and the formation of the shadow cast by a Bonnor black dihole. Finally, we present a summary.

II. SPACETIME OF A BONNOR BLACK DIHOLE AND NULL GEODESICS

Let us now briefly review the spacetime of a Bonnor black dihole. In the 1960s, Bonnor obtained an exact solution [41] of the Einstein-Maxwell equations that describes a static massive source carrying a magnetic dipole. In the standard coordinates, the metric of this spacetime has the form [41]

$$ds^2 = -\left(\frac{P}{Y}\right)^2 dt^2 + \frac{P^2Y^2}{Q^3Z}(dr^2 + Zd\theta^2) + \frac{Y^2Z\sin^2\theta}{P^2}d\phi^2, \tag{1}$$

where

$$P = r^2 - 2mr - b^2\cos^2\theta,$$
$$Q = (r-m)^2 - (m^2+b^2)\cos^2\theta, \qquad Y = r^2 - b^2\cos^2\theta,$$
$$Z = r^2 - 2mr - b^2. \tag{2}$$

The corresponding vector potential A_μ is given by

$$A_\mu = \left(0, 0, 0, \frac{2mbr\sin^2\theta}{P}\right), \tag{3}$$

where $\mu = 0, 1, 2, 3$ correspond to the elements of A_μ associated with the coordinates t, r, θ, ϕ, respectively. It is a static axially symmetric solution characterized by two independent parameters m and b, which are related to the total mass of the Bonnor black dihole M by $M = 2m$ and to the magnetic dipole moment μ by $\mu = 2mb$. Obviously, this spacetime is asymptotically flat since when the polar coordinate r approaches infinity, the metric tends to the Minkowski one. The event horizon of the spacetime (1) is the null hypersurface f that satisfies

$$g^{\mu\nu}\frac{\partial f}{\partial x^\mu}\frac{\partial f}{\partial x^\nu} = 0, \tag{4}$$

which yields

$$r^2 - 2mr - b^2 = 0. \tag{5}$$

It is obvious that there exists only a horizon, and the corresponding horizon radius is $r_h = m + \sqrt{m^2+b^2}$. The area of the horizon is $\mathcal{A} = 16\pi m^2 r_h^2/(m^2+b^2)$, but the proper circumference of the horizon surface is zero since $g_{\phi\phi} = 0$ on the horizon. This implies that the $Z = 0$ surface is not a regular horizon since there exist conical singularities at $r = r_h$. The singularity along the segment $r = r_h$ can be eliminated by selecting a proper period $\Delta\phi = 2\pi[b^2/(m^2+b^2)]^2$, but such a choice yields a conical deficit running along the axes $\theta = 0, \pi$, from the end points of the dipole to infinity [45,46]. The defects outside of the dipole can be treated as open cosmic strings, and then the Bonnor black dihole is held apart by the cosmic strings that pull from its end points. Since the angular coordinate ϕ is periodic, an azimuthal curve $\gamma = \{t = \text{const}, r = \text{const}, \theta = \text{const}\}$ is a closed curve with invariant length $s_\gamma^2 = g_{\phi\phi}(2\pi)^2$. Then, the integral curve with (t, r, θ) fixed is a closed timelike curve when $g_{\phi\phi} < 0$. Thus, there exist closed timelike curves inside the horizon. However, the region outside the horizon is regular and there are no closed timelike curves. Moreover, the spacetime (1) possesses a complicated singular behavior at $P = 0$, $Q = 0$, and $Y = 0$, but there is no singularity outside the horizon. When $b = 0$, one can find that it does not reduce to the Schwarzschild spacetime, but rather to the Zipoy-Voorhees one with $\delta = 2$ [47,48], which describes a monopole of mass $2m$ together with higher-mass multipoles that depend on the parameter m. These special spacetime properties affect the propagation of photons and further change the shadow of the Bonnor black dihole (1).

The Hamiltonian of photon motion along null geodesics in the spacetime (1) can be expressed as

$$H(x,p)=\frac{1}{2}g^{\mu\nu}(x)p_\mu p_\nu=0. \tag{6}$$

Since the metric functions in the spacetime (1) are independent of the coordinates t and ϕ, it is easy to obtain two conserved quantities E and L_z with the following forms:

$$E=-p_t=-g_{00}\dot{t}, \qquad L_z=p_\phi=g_{33}\dot{\phi}, \tag{7}$$

which correspond to the energy and the z component of the angular momentum of a photon moving in the background spacetime. With these two conserved quantities, we can obtain the equations of photon motion along null geodesics:

$$\begin{aligned}
\ddot{r}=&-\frac{1}{2}\frac{\partial}{\partial r}\left[\ln\left(\frac{P^2Y^2}{Q^3Z}\right)\right]\dot{r}^2-\frac{\partial}{\partial\theta}\left[\ln\left(\frac{P^2Y^2}{Q^3Z}\right)\right]\dot{r}\dot{\theta}+\frac{Z}{2}\frac{\partial}{\partial r}\left[\ln\left(\frac{P^2Y^2}{Q^3}\right)\right]\dot{\theta}^2\\
&-\frac{Q^3Z}{2}\left[\frac{E^2}{P^4}\frac{\partial}{\partial r}\ln\left(\frac{P^2}{Y^2}\right)-\frac{L_z^2}{Y^4Z\sin\theta}\frac{\partial}{\partial r}\ln\left(\frac{Y^2Z\sin\theta}{P^2}\right)\right],\\
\ddot{\theta}=&\frac{1}{2Z}\frac{\partial}{\partial\theta}\left[\ln\left(\frac{P^2Y^2}{Q^3}\right)\right]\dot{r}^2-\frac{\partial}{\partial r}\left[\ln\left(\frac{P^2Y^2}{Q^3Z}\right)\right]\dot{r}\dot{\theta}+\frac{1}{2}\frac{\partial}{\partial\theta}\left[\ln\left(\frac{P^2Y^2}{Q^3}\right)\right]\dot{\theta}^2\\
&-\frac{Q^3}{2}\left[\frac{E^2}{P^4}\frac{\partial}{\partial\theta}\ln\left(\frac{P^2}{Y^2}\right)-\frac{L_z^2}{Y^4Z\sin\theta}\frac{\partial}{\partial\theta}\ln\left(\frac{Y^2Z\sin\theta}{P^2}\right)\right],
\end{aligned} \tag{8}$$

with the constraint condition

$$H=\frac{1}{2}\left(\frac{Q^3Z}{P^2Y^2}p_r^2+\frac{Q^3}{P^2Y^2}p_\theta^2+V\right)=0, \tag{9}$$

where p_r and p_θ are the components of the momentum of the photon $p_r=g_{11}\dot{r}$ and $p_\theta=g_{22}\dot{\theta}$. V is the effective potential with the form

$$V=-\left(\frac{Y}{P}\right)^2E^2+\frac{P^2}{Y^2Z\sin^2\theta}L_z^2. \tag{10}$$

Obviously, in the case with a magnetic dipole (i.e., $b\neq 0$), we find that the equations of motion (8)–(9) cannot be variable separable, and the corresponding dynamical system is nonintegrable because it admits only two integrals of motion E and L_z. This implies that the motion of the photon could be chaotic in the spacetime (1), which will give rise to some new features for the shadow cast by a Bonnor black dihole.

III. SHADOW CAST BY A BONNOR BLACK DIHOLE

In this section, we will study the shadow cast by a Bonnor black dihole with the method called "backward ray tracing" [24–27] in which the light rays are assumed to evolve from the observer backward in time. In this method, we must numerically solve the null geodesic equations (7) and (8) for each pixel in the final image with the corresponding initial condition. The image of a shadow in the observer's sky is composed of the pixels corresponding to the light rays falling down into the horizon of the black hole.

Since the spacetime of a Bonnor black dihole (1) is asymptotically flat, we can define the same observer's sky at spatial infinity as in the usual static cases. The observer basis $\{e_{\hat{t}},e_{\hat{r}},e_{\hat{\theta}},e_{\hat{\phi}}\}$ can be expanded in the coordinate basis $\{\partial_t,\partial_r,\partial_\theta,\partial_\phi\}$ in the form [24–27]

$$e_{\hat{\mu}}=e^\nu_{\hat{\mu}}\partial_\nu, \tag{11}$$

where $e^\nu_{\hat{\mu}}$ satisfies $g_{\mu\nu}e^\mu_{\hat{\alpha}}e^\nu_{\hat{\beta}}=\eta_{\hat{\alpha}\hat{\beta}}$, and $\eta_{\hat{\alpha}\hat{\beta}}$ is the usual Minkowski metric. For a static spacetime, it is convenient to choose the decomposition

$$e^\nu_{\hat{\mu}}=\begin{pmatrix}\zeta & 0 & 0 & 0\\ 0 & A^r & 0 & 0\\ 0 & 0 & A^\theta & 0\\ 0 & 0 & 0 & A^\phi\end{pmatrix}, \tag{12}$$

where ζ, A^r, A^θ, and A^ϕ are real coefficients. From the Minkowski normalization, one can find that the observer basis obeys

$$e_{\hat{\mu}}e^{\hat{\nu}}=\delta^{\hat{\nu}}_{\hat{\mu}}. \tag{13}$$

Therefore, we have

$$\zeta=\frac{1}{\sqrt{-g_{00}}}, \quad A^r=\frac{1}{\sqrt{g_{11}}}, \quad A^\theta=\frac{1}{\sqrt{g_{22}}}, \quad A^\phi=\frac{1}{\sqrt{g_{33}}}, \tag{14}$$

and then the locally measured four-momentum $p^{\hat{\mu}}$ of a photon can be obtained by the projection of its four-momentum p^μ onto $e_{\hat{\mu}}$,

$$p^{\hat{t}}=-p_{\hat{t}}=-e^\nu_{\hat{t}}p_\nu, \qquad p^{\hat{i}}=p_{\hat{i}}=e^\nu_{\hat{i}}p_\nu. \tag{15}$$

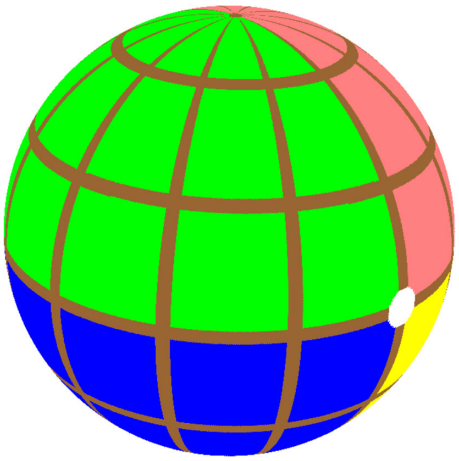

FIG. 1. The sphere light source marked by four different-colored quadrants and the brown grids of longitude and latitude. The white reference spot lies at the intersection of the four colored quadrants.

In the spacetime of a Bonnor black dihole (1), the locally measured four-momentum $p^{\hat{\mu}}$ can be further written as

$$p^{\hat{t}} = \frac{1}{\sqrt{-g_{00}}}E, \qquad p^{\hat{r}} = \frac{1}{\sqrt{g_{11}}}p_r,$$
$$p^{\hat{\theta}} = \frac{1}{\sqrt{g_{22}}}p_\theta, \qquad p^{\hat{\phi}} = \frac{1}{\sqrt{g_{33}}}L_z. \tag{16}$$

After some similar operations as in Refs. [24–27], we can obtain the position of a photon's image in the observer's sky [5],

$$x = -r_{\rm obs}\frac{p^{\hat{\phi}}}{p^{\hat{r}}} = -r_{\rm obs}\frac{L_z}{\sqrt{g_{11}g_{33}}\dot{r}},$$
$$y = r_{\rm obs}\frac{p^{\hat{\theta}}}{p^{\hat{r}}} = r_{\rm obs}\frac{\sqrt{g_{22}}\dot{\theta}}{\sqrt{g_{11}}\dot{r}}. \tag{17}$$

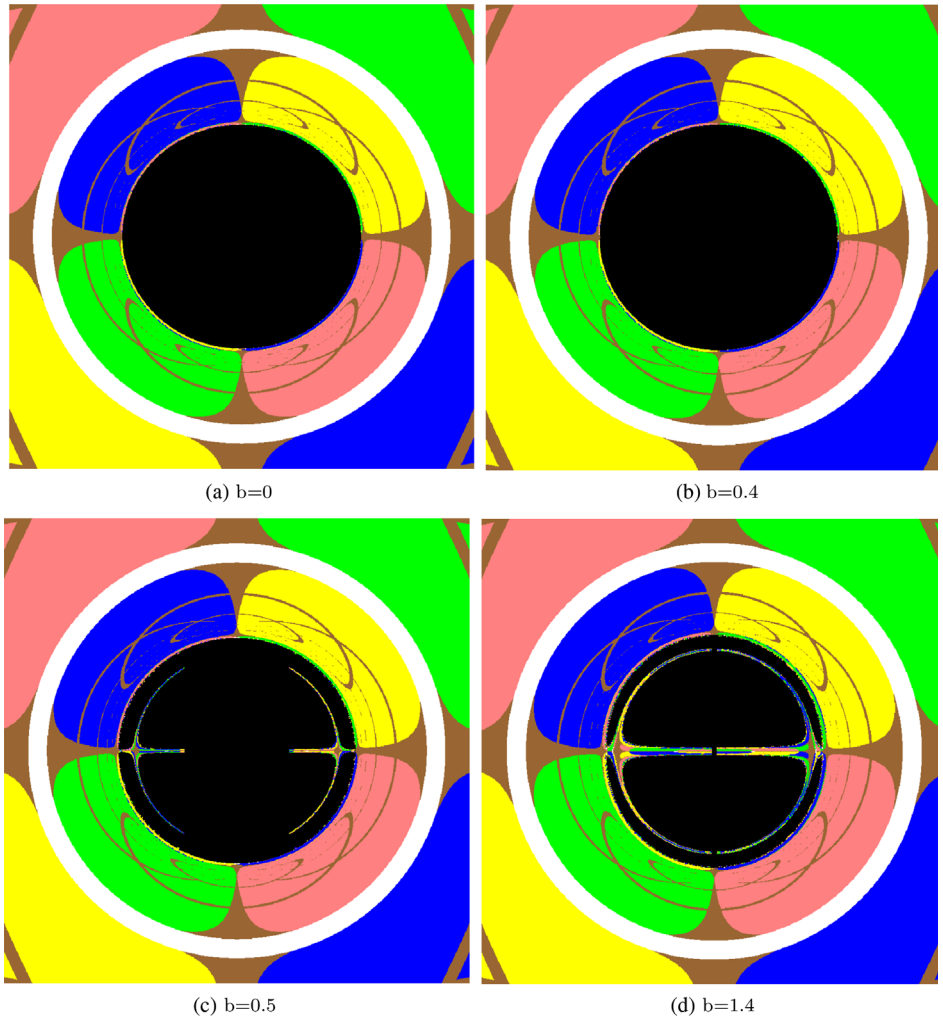

(a) b=0 (b) b=0.4

(c) b=0.5 (d) b=1.4

FIG. 2. The shadow cast by a Bonnor black dihole (1) with different b. Here we set $m = 1$ and the observer is set at $r_{\rm obs} = 30m$ with the inclination angle $\theta_0 = 90°$.

Following Refs. [24–29], one can divide the celestial sphere into four quadrants marked by different colors (green, blue, red, and yellow, as shown in Fig. 1). The grid of longitude and latitude lines is marked with adjacent brown lines separated by 10°. The observer is placed off-center within the celestial sphere at some real radius $r_{\rm obs}$. For the sake of simplicity, it is placed at the intersection of the four colored quadrants on the celestial sphere, i.e., $r_{\rm obs} = r_{\rm sphere}$, which is not shown in Fig. 1. The white reference spot in Fig. 1 lies at the other intersection of the four colored quadrants, which could provide a direct demonstration of an Einstein ring [24–29]. We can integrate these null geodesics with different initial conditions until they either reach a point on the celestial sphere or they fall into the horizon of the compact object, and the latter defines the shadow. In Fig. 2, we present the shadow cast by a Bonnor black dihole (1) with different b. Here we set $m = 1$ and the observer is set at $r_{\rm obs} = 30m$ with the inclination angle $\theta_0 = 90°$. Our numerical results show that there exists a critical value $b_c \sim 0.404$ for the shadow. When $b < b_c$, we find that the shadow is a black disk, which is similar to those in the usual static compact object spacetimes with a horizon. Moreover, we find that the size of the shadow decreases with the parameter b in this case. However, for the case $b > b_c$, there exist two anchor-like bright zones embedded symmetrically in the black disk shadow so that the shadow looks like a concave disk with four larger eyebrows, which are shown in Figs. 2(c) and 2(d). The eyebrow-like features of the shadow were also found in Refs. [24–29]. Actually, many other smaller eyebrow-like shadows can be detected in two anchor-like bright zones, as shown in Fig. 3. This hints that the shadow possesses a self-similar fractal structure, which is caused by chaotic lensing. It is an interesting property of shadows, which is qualitatively different from those in spacetimes where the equations of motion are variable separable and the

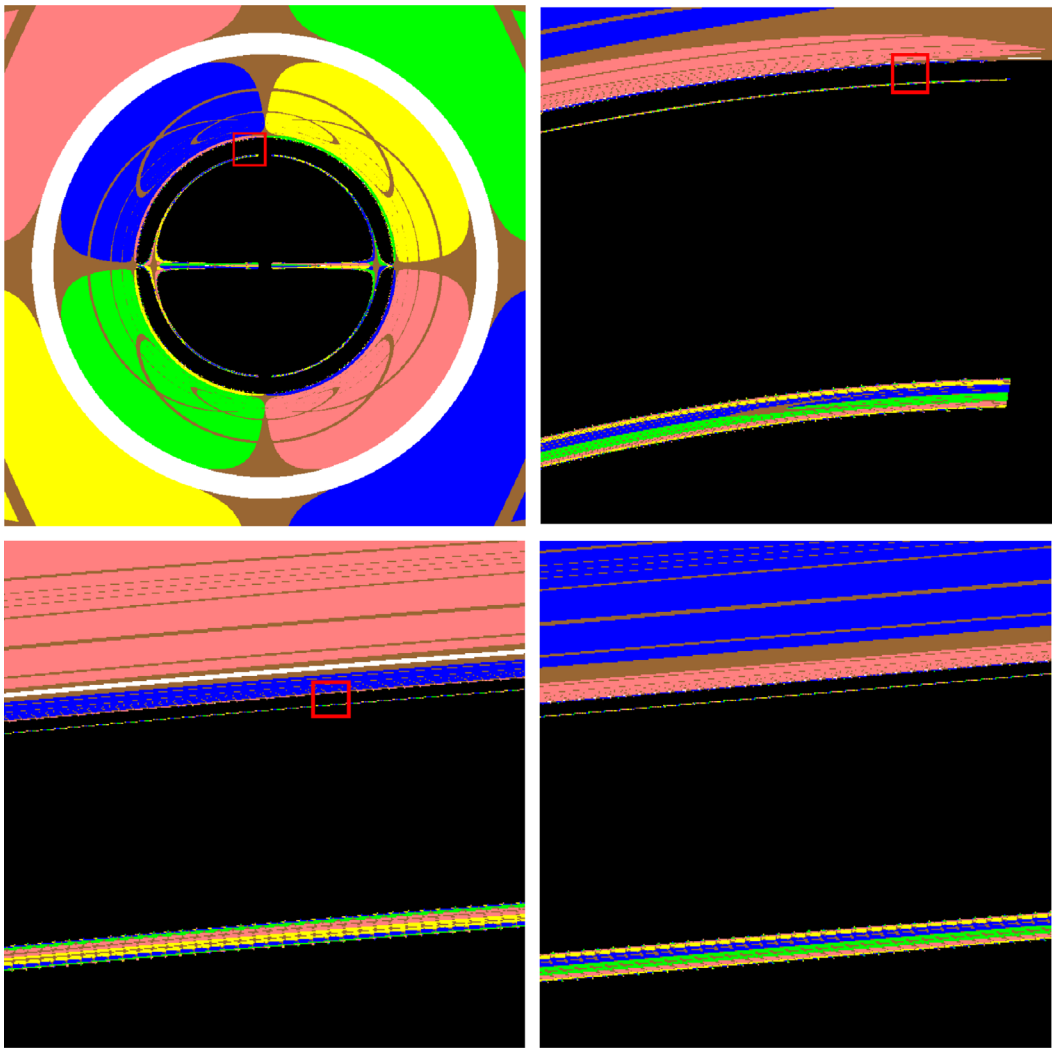

FIG. 3. The fractal structure in the shadow of a Bonnor black dihole (1) for fixed $b = 1.0$. Here we set $m = 1$ and the observer is set at $r_{\rm obs} = 30m$ with the inclination angle $\theta_0 = 90°$.

corresponding dynamical system is integrable. With the increase of the magnetic dipole parameter b, the eyebrows become long and the fractal structure becomes more rich. Moreover, we find that the two anchor-like bright zones increase with the parameter b, but for arbitrary b, the two anchor-like bright zones are disconnected since they are always separated by a black region. In other words, for a Bonnor black dihole, the two larger shadows and the smaller eyebrow-like shadows are joined together by the middle black zone. Moreover, the white circle in Figs. 2 and 3 denote an Einstein ring, which is consistent with the prediction of multiple images of a source due to gravitational lensing.

IV. INVARIANT PHASE-SPACE STRUCTURES AND THE FORMATION OF A SHADOW CAST BY A BONNOR BLACK DIHOLE

In this section, we will discuss the formation of the shadow cast by a Bonnor black dihole by analyzing the invariant phase-space structures as in Ref. [30]. The invariant phase-space structures—including fixed points, periodic orbits, and invariant manifolds—are important features for dynamical systems, which are applied extensively in the design of space trajectories for various types of spacecraft, such as low-energy transfer from the Earth to the Moon and a "Petit Grand Tour" of the moons of Jupiter [49–53]. Recent investigations [30] have shown that these invariant structures play an important role in the emergence of black hole shadows.

For the spacetime of a Bonnor black dihole (1), the fixed point $x_0 = (r_0, \theta_0, 0, 0)$ in phase space $(r, \theta, p_r, p_\theta)$ satisfies the condition

$$\dot{x}^\mu = \frac{\partial H}{\partial p_\mu} = 0, \qquad \dot{p}_\mu = -\frac{\partial H}{\partial x^\mu} = 0, \tag{18}$$

which means

$$V|_{r_0,\theta_0} = 0, \qquad \left.\frac{\partial V}{\partial r}\right|_{r_0,\theta_0} = 0, \qquad \left.\frac{\partial V}{\partial \theta}\right|_{r_0,\theta_0} = 0. \tag{19}$$

The local stability of the fixed point $x_0 = (r_0, \theta_0, 0, 0)$ can be obtained by linearizing the Eq. (18),

$$\dot{\mathbf{X}} = J\mathbf{X}, \tag{20}$$

where $\mathbf{X} = (\tilde{x}^\mu, \tilde{p}_\mu)$ and J is the Jacobian. The circular photon orbits in the equatorial plane (called light rings) are fixed points of the dynamics of photon motion [4,30]. After linearizing the Eq. (18) near the fixed point $(r_0, \pi/2, 0, 0)$ and setting $m = 1$, we obtain the Jacobian

$$J = \begin{bmatrix} 0 & 0 & 2A & 0 \\ 0 & 0 & 0 & 2B \\ -2C & 0 & 0 & 0 \\ 0 & -2D & 0 & 0 \end{bmatrix}, \tag{21}$$

with

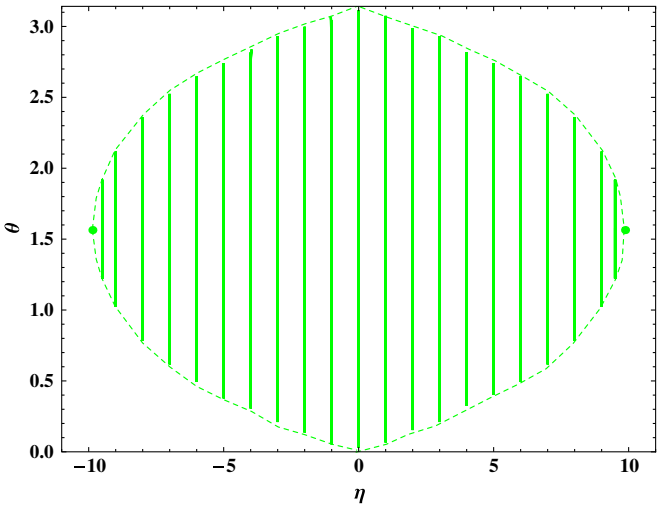

FIG. 4. Light rings (dots) and the corresponding family of periodic Lyapunov orbits (solid line) in the spacetime of a Bonnor black dihole with $b = 1.4$. Here we set $m = 1$.

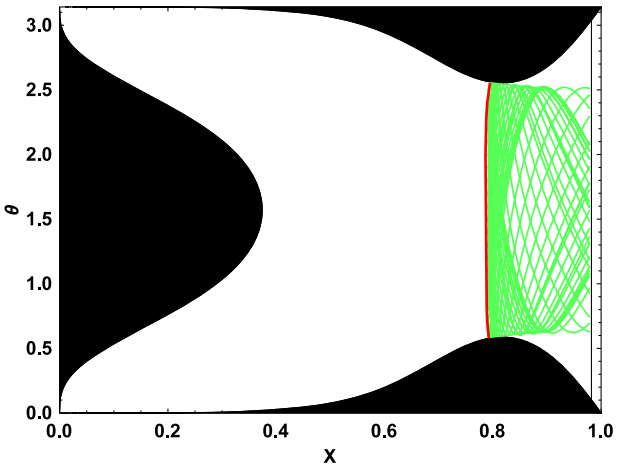

FIG. 5. Projection of the unstable invariant manifolds (green lines) associated with the periodic orbit for $\eta = -6$ (red line). The dark regions are the forbidden regions for photons and the black dot represents the position of the observer.

$$A=\frac{(r_0-1)^6(r_0^2-2r_0-b^2)}{r_0^6(r_0-2)^2},$$

$$B=\frac{(r_0-1)^6}{r_0^6(r_0-2)^2},$$

$$C=\frac{\eta^2[3r_0^2(r_0-4)(r_0-2)^3+b^2r_0(r_0-2)^2(16+r_0)-4b^4(r_0-3)]}{r_0^4(r_0^2-2r_0-b^2)^3}-4\frac{r_0+1}{(r_0-2)^4},$$

$$D=\frac{\eta^2(r_0-2)(r_0^3-2r_0^2-4b^2)}{r_0^4(r_0^2-2r_0-b^2)}-\frac{4b^2}{(r_0-2)^3},$$

$$r_0=\frac{1}{3}\left[(3\sqrt{3}\sqrt{108b^4-112b^2-225}-54b^2+28)^{1/3}+7+\frac{19}{(3\sqrt{3}\sqrt{108b^4-112b^2-225}-54b^2+28)^{1/3}}\right], \quad (22)$$

where $\eta\equiv L_z/E$.

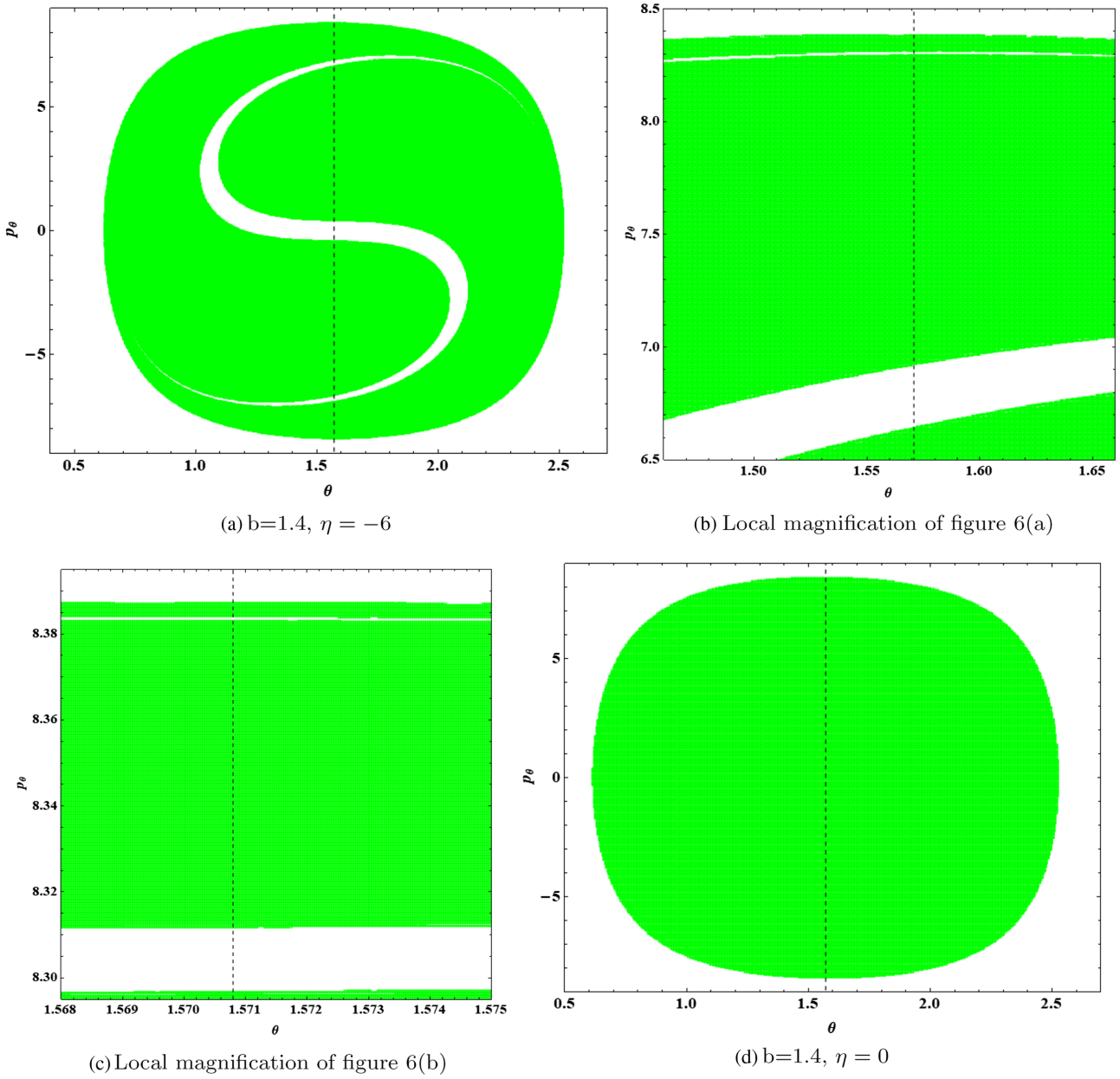

(a) b=1.4, $\eta=-6$

(b) Local magnification of figure 6(a)

(c) Local magnification of figure 6(b)

(d) b=1.4, $\eta=0$

FIG. 6. The Poincaré section at $r=r_{\rm obs}$ for the unstable manifolds (green) of Lyapunov orbits in the spacetime of a Bonnor black dihole (1) with $b=1.4$. Panels (a)–(c) show the fractal-like structure for $\eta=-6$, and panel (d) is for $\eta=0$. Here we set $m=1$.

Let us now adopt the case $m = 1$ and $b = 1.4$ as an example to analyze the formation of the shadow of a Bonnor black dihole (1), which is shown in Fig. 2(d). In this special case, we find that there exist two fixed points. Their positions in phase space overlap at $(4.07, \pi/2, 0, 0)$, but their impact parameters are $\eta_1 = -9.83$ and $\eta_2 = 9.83$, respectively. The special distribution of the two fixed points is attributed to the fact that the considered magnetic dipole spacetime (1) is a nonrotating spacetime. The eigenvalues of the Jacobian (21) are $\pm\lambda$, $\pm\nu i$, where $\lambda = 0.46$ and $\nu = 0.60$. According to Lyapunov's central limit theorem, we know that each purely imaginary eigenvalue gives rise to a one-parameter family γ_ϵ of periodic orbits (which is the so-called Lyapunov family [30]), and the orbit γ_ϵ collapses into the fixed point as $\epsilon \to 0$. We show the Lyapunov family for the above fixed points (light rings) in Fig. 4. The two thick dots represent the two light rings, and the solid lines denote a family of periodic Lyapunov orbits arising from these two light rings. These periodic orbits can be parametrized by the impact parameter η on the interval $[-9.83, 9.83]$. All of these periodic Lyapunov orbits are nearly spherical orbits with radius $r = 4.07$, which are responsible for determining the boundary of the shadow of a Bonnor black dihole, as in Refs. [4,30]. The positive (negative) real eigenvalue $\pm\lambda$ suggests that there is an unstable (stable) invariant manifold, in which points exponentially approach the fixed point backward (forward) time. For each Lyapunov orbit, its corresponding invariant manifolds are two-dimensional surfaces forming tubes in the three-dimensional reduced phase space $(r; \theta; p_\theta)$. In Fig. 5, we show a projection of the unstable invariant manifolds associated with the periodic orbits for $\eta = -6$ in the plane (X, θ), where X is a compactified radial coordinate defined as $X = \sqrt{r^2 - r_h^2}/(1 + \sqrt{r^2 - r_h^2})$ [30]. The orbits inside the unstable invariant manifold tube can reach the horizon of a Bonnor black dihole. Moreover, we note that the periodic orbit that touches the boundary of the black region approaches the boundary $V(r, \theta) = 0$ perpendicularly, as in Ref. [28].

In order to probe the shape of the invariant manifolds as in Ref. [30], we present in Fig. 6 the Poincaré section in the plane (θ, p_θ) for the unstable manifolds of Lyapunov orbits at the observer's radial position with $\eta = -6$ and $\eta = 0$. All photons that start within the green regions always move only in the unstable manifold tube. Moreover, we also note that there exist some white regions which correspond to where photons move outside the unstable manifolds. In Fig. 6, the intersection of the dashed line $\theta = \frac{\pi}{2}$ with these manifolds denotes the trajectories which can be detected by the observer on the equatorial plane. This can be generalized to cases with other values of θ. Actually, these intersection points also determine the positions of the photons with a certain angular momentum on the image plane. In Fig. 7, we present the lensing image marking the intersection points for fixed $\eta = -9.83$, $\eta = -6$, and $\eta = 0$.

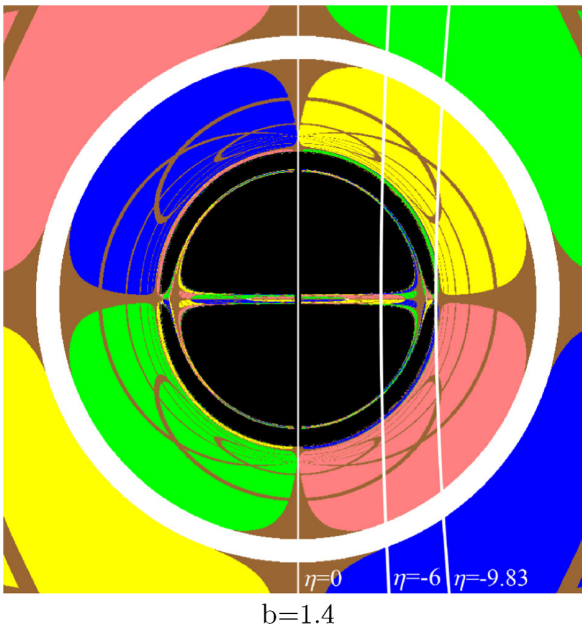

FIG. 7. Intersections of the unstable manifolds with the image plane for the lines with constant $\eta = -9.83$, $\eta = -6$, and $\eta = 0$ in the spacetime of a Bonnor black dihole (1) with $b = 1.4$.

The boundary of the shadow of a Bonnor black dihole is entirely determined by the intersection points deriving from these fixed points. The anchor-like bright zones in Fig. 2(d) come from the top, middle, and bottom parts of the S-shaped white region in the Poincaré section [see Fig. 6(a)], and the fractal-like structure shown in Figs. 6(a)–6(c) is responsible for the fractal shadow structure in Fig. 3. For the case $\eta = 0$, there is no white region in the Poincaré section [see Fig. 6(d)], which is responsible for the fact that the two anchor-like bright zones are separated by the black shadow in the middle regions in Fig. 2(d). In order to make a comparison, in Fig. 8, we also plot the Poincaré section and the intersections of the unstable manifolds with the image plane for $\eta = -6$ in the spacetime of a Bonnor black dihole (1) with $b = 0.4$. Obviously, there is no white region in the Poincaré section, which is consistent with the fact that the shadow of a Bonnor black dihole is a black disk and there are no bright zones in the shadow in this case.

Finally, we make a comparison between the shadows cast by the equal-mass and nonspinning Majumdar-Papapetrou binary black holes [28,29] and by a Bonnor black dihole (1). In Fig. 9, we present the shadow for Majumdar-Papapetrou binary black holes [28,29] with two equal-mass black holes separated by the parameter $a = 0.5$, $a = 1$, and $a = 2$ [Figs. 9(a)–9(c)] and for the cases of a Bonnor black dihole (1) separated by the parameter $b = 0.5$, $b = 1$, and $b = 2$ [Figs. 9(d)–9(f)]. From Fig. 9, one can find that the shadows of a Bonnor black dihole possess some properties that closely resemble those of Majumdar-Papapetrou binary black holes, which is understandable since similar black hole configurations

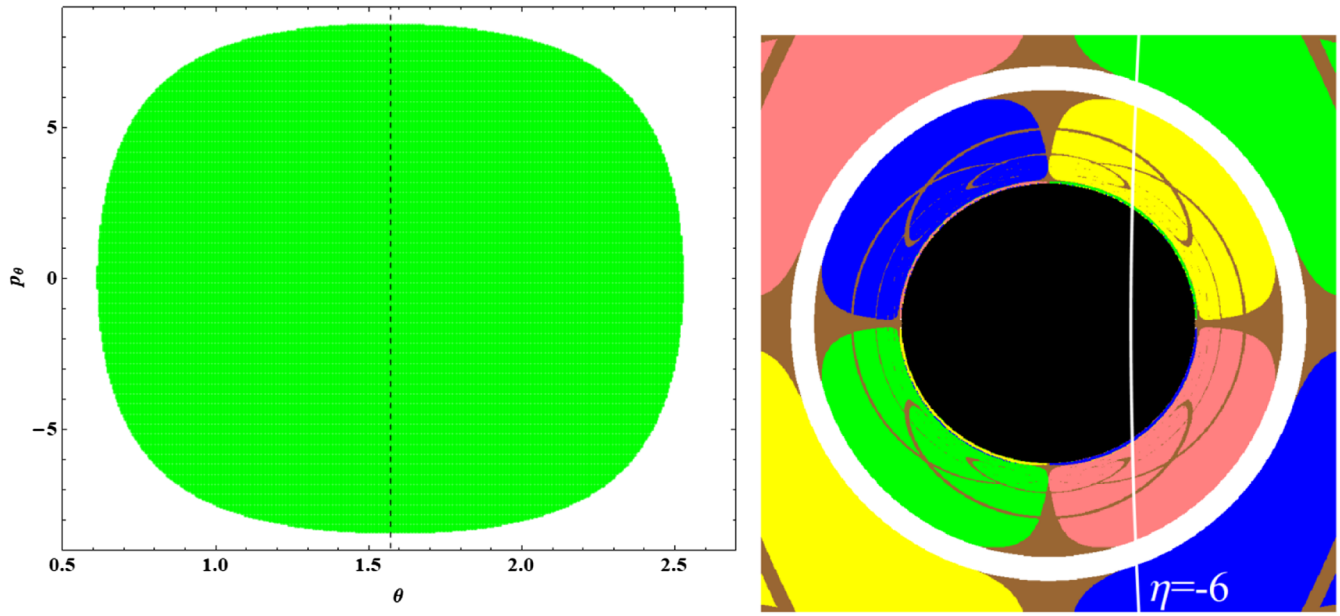

(a) b=0.4, $\eta = -6$ (b) b=0.4

FIG. 8. The Poincaré section (left) and the intersections of the unstable manifolds with the image plane (right) for $\eta = -6$ in the spacetime of a Bonnor black dihole (1) with $b = 0.4$.

exist in both cases. However, there is an essential difference between the shadows for a given parameter in these two cases. From Fig. 9, we find that the two larger shadows and the smaller eyebrow-like shadows are joined together by the middle black zone for a Bonnor black dihole, but they are disconnected in the case of the equal-mass and nonspinning Majumdar-Papapetrou binary black holes [28,29]. Moreover, with the increase of the magnetic dipole

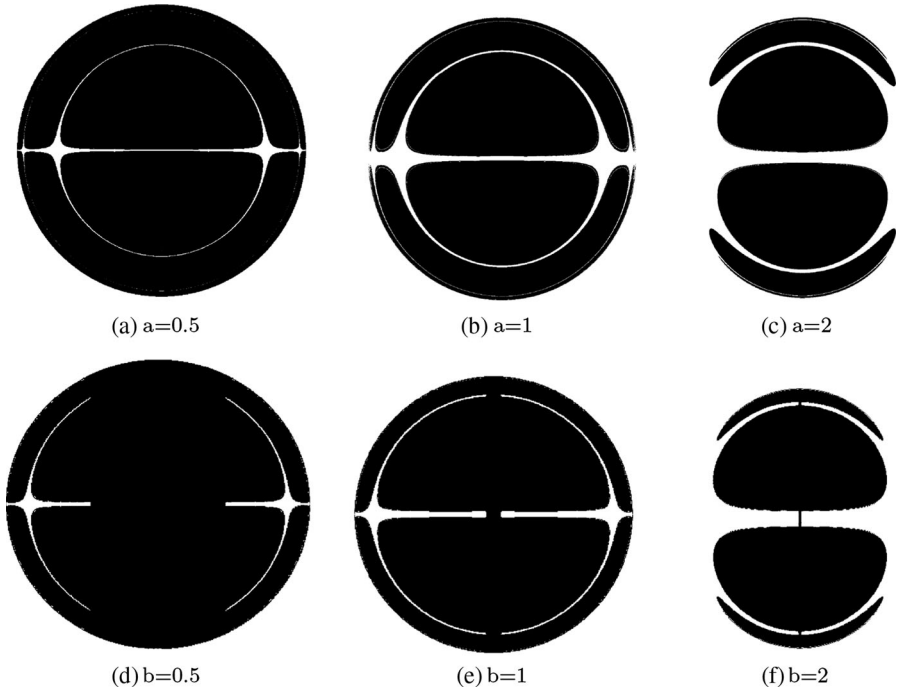

(a) a=0.5 (b) a=1 (c) a=2

(d) b=0.5 (e) b=1 (f) b=2

FIG. 9. Comparison between the shadows of Majumdar-Papapetrou binary black holes and a Bonnor black dihole (1). Panels (a)–(c) correspond to the Majumdar-Papapetrou binary case [28,29] with two equal-mass black holes separated by the parameter $a = 0.5$, $a = 1$, and $a = 2$, respectively. Panels (d)–(f) denote the shadow for the cases of a Bonnor black dihole (1) separated by the parameter $b = 0.5$, $b = 1$, and $b = 2$, respectively. Here we set the inclination angle of the observer $\theta_0 = 90°$ and $m = 1$.

parameter, we find that the middle black zone connecting the main shadows and the eyebrow-like shadows becomes narrow for a Bonnor black dihole. From the previous discussion, we know that due to the existence of the singularity on the symmetric axis, a Bonnor black dihole is held apart by the cosmic string with tension $\mu = \frac{1}{4}[1 - b^4/(m^2 + b^2)^2]$ [45,46], which decreases with the parameter b. Therefore, we can obtain that the middle black zone increases with the tension of the cosmic string. This behavior is consistent with that in the case of a Kerr black hole pierced by a cosmic string, in which the size of the black hole shadow increases with the string tension [16]. Therefore, the appearance of the middle black zone in the shadow of a Bonnor black dihole can be attributed to the existence of the conical singularity on the symmetric axis in the background spacetime. In the case of Majumdar-Papapetrou binary black holes [28,29], there is no such conical singularity since the configuration is supported by the balance between the gravitational force and the Coulomb force. Thus, the difference in the shape of the shadow in these two spacetimes is caused by the existence of the singularity on the symmetric axis in Bonnor's spacetime.

V. SUMMARY

In this paper we have studied the shadows of a black dihole described by Bonnor's exact solution of the Einstein-Maxwell equations. The presence of a magnetic dipole yields that the equation of photon motion can not be variable separable and the corresponding dynamical system is nonintegrable. With the technique of backward ray tracing, we numerically presented the shadow of a Bonnor black dihole. For the smaller magnetic dipole parameter b, the shadow is a black disk as in the usual static compact object spacetimes with a horizon. The size of the shadow decreases with the parameter b. For the larger magnetic dipole parameter b, we found that there exist two anchor-like bright zones embedded symmetrically in the black disk shadow so that the shadow looks like a concave disk with four large eyebrows. The anchor-like bright zones increase and the eyebrows become longer with the increase of b. Moreover, many other smaller eyebrow-like shadows can be detected in two anchor-like bright zones and the shadow possesses a self-similar fractal structure, which is caused by chaotic lensing. This interesting property of shadows is qualitatively different from those in the spacetimes in which the equations of motion are variable separable and the corresponding dynamical system is integrable. Finally, we analyzed the invariant manifolds of certain Lyapunov orbits near the fixed point and further discussed the formation of the shadow of a Bonnor black dihole, which indicates that all of the structures in the shadow originate naturally from the dynamics near fixed points. Our results show that the spacetime properties arising from the magnetic dipole give rise to some interesting patterns for the shadow cast by a Bonnor black dihole.

Comparing with the case of Majumdar-Papapetrou binary black holes, we found that the two larger shadows and the smaller eyebrow-like shadows are joined together by the middle black zone for a Bonnor black dihole, but they are disconnected in the Majumdar-Papapetrou one. The appearance of the middle black zone in the shadow of a Bonnor black dihole can be attributed to the existence of the conical singularity on the symmetric axis in the background spacetime. It is of interest to study the effects of such a conical singularity on the Lyapunov orbits and the shadow's edge, etc. Work in this direction will be reported in the future [54].

ACKNOWLEDGMENTS

We wish to thank anonymous referees very much for their useful comments and suggestions, which improved our paper considerably. This work was partially supported by the Scientific Research Fund of Hunan Provincial Education Department Grant No. 17A124. J. J.'s work was partially supported by the National Natural Science Foundation of China under Grant No. 11475061.

[1] J. L. Synge, The escape of photons from gravitationally intense stars, Mon. Not. R. Astron. Soc. **131**, 463 (1966).
[2] J. M. Bardeen, in *Black Holes (Les Astres Occlus)*, edited by C. DeWitt and B. DeWitt (Gordon and Breach, New York, 1973), p. 215.
[3] S. Chandrasekhar, *The Mathematical Theory of Black Holes* (Oxford University, New York, 1992).
[4] P. V. P. Cunha, C. Herdeiro, and E. Radu, Fundamental photon orbits: black hole shadows and spacetime instabilities, Phys. Rev. D **96**, 024039 (2017).
[5] M. Wang, S. Chen, and J. Jing, Shadow casted by a Konoplya-Zhidenko rotating non-Kerr black hole, J. Cosmol. Astropart. Phys. 10 (2017) 051.
[6] H. Falcke, F. Melia, and E. Agol, Viewing the shadow of the black hole at the Galactic center, Astrophys. J. **528**, L13 (2000).

[7] A. de Vries, The apparent shape of a rotating charged black hole, closed photon orbits and the bifurcation set A_4, Classical Quantum Gravity **17**, 123 (2000).
[8] R. Takahashi, Shapes and positions of black hole shadows in accretion disks and spin parameters of black holes, Astrophys. J. **611**, 996 (2004).
[9] C. Bambi and K. Freese, Apparent shape of super-spinning black holes, Phys. Rev. D **79**, 043002 (2009); Z. Li and C. Bambi, Measuring the Kerr spin parameter of regular black holes from their shadow, J. Cosmol. Astropart. Phys. 01 (2014) 041.
[10] K. Hioki and K. I. Maeda, Measurement of the Kerr spin parameter by observation of a compact object's shadow, Phys. Rev. D **80**, 024042 (2009).
[11] L. Amarilla, E. F. Eiroa, and G. Giribet, Null geodesics and shadow of a rotating black hole in extended Chern-Simons modified gravity, Phys. Rev. D **81**, 124045 (2010).
[12] L. Amarilla and E. F. Eiroa, Shadow of a rotating brane-world black hole, Phys. Rev. D **85**, 064019 (2012).
[13] A. Yumoto, D. Nitta, T. Chiba, and N. Sugiyama, Shadows of multi-black holes: Analytic exploration, Phys. Rev. D **86**, 103001 (2012).
[14] L. Amarilla and E. F. Eiroa, Shadow of a Kaluza-Klein rotating dilaton black hole, Phys. Rev. D **87**, 044057 (2013).
[15] P. G. Nedkova, V. Tinchev, and S. S. Yazadjiev, The shadow of a rotating traversable wormhole, Phys. Rev. D **88**, 124019 (2013).
[16] V. K. Tinchev and S. S. Yazadjiev, Possible imprints of cosmic strings in the shadows of galactic black holes, Int. J. Mod. Phys. D **23**, 1450060 (2014).
[17] S. W. Wei and Y. X. Liu, Observing the shadow of Einstein-Maxwell-dilaton-axion black hole, J. Cosmol. Astropart. Phys. 11 (2013) 063.
[18] V. Perlick, O. Y. Tsupko, and G. S. Bisnovatyi-Kogan, Influence of a plasma on the shadow of a spherically symmetric black hole, Phys. Rev. D **92**, 104031 (2015).
[19] Y. Huang, S. Chen, and J. Jing, Double shadow of a regular phantom black hole as photons couple to Weyl tensor, Eur. Phys. J. C **76**, 594 (2016).
[20] Z. Younsi, A. Zhidenko, L. Rezzolla, R. Konoplya, and Y. Mizuno, A new method for shadow calculations: application to parameterised axisymmetric black holes, Phys. Rev. D **94**, 084025 (2016).
[21] A. Abdujabbarov, M. Amir, B. Ahmedov, and S. Ghosh, Shadow of rotating regular black holes, Phys. Rev. D **93**, 104004 (2016); A. Abdujabbarov, L. Rezzolla, and B. Ahmedov, A coordinate-independent characterization of a black hole shadow, Mon. Not. R. Astron. Soc. **454**, 2423 (2015); F. Atamurotov, B. Ahmedov, and A. Abdujabbarov, Optical properties of black holes in the presence of a plasma: The shadow, Phys. Rev. D **92**, 084005 (2015); A. Abdujabbarov, F. Atamurotov, N. Dadhich, B. Ahmedov, and Z. Stuchlík, Energetics and optical properties of 6-dimensional rotating black hole in pure Gauss-Bonnet gravity, Eur. Phys. J. C **75**, 399 (2015); F. Atamurotov, A. Abdujabbarov, and B. Ahmedov, Shadow of rotating non-Kerr black hole, Phys. Rev. D **88**, 064004 (2013).
[22] N. Tsukamoto, Black hole shadow in an asymptotically-flat, stationary, and axisymmetric spacetime: The Kerr-Newman and rotating regular black holes, Phys. Rev. D **97**, 064021 (2018).
[23] P. V. P. Cunha and C. A. R. Herdeiro, Shadows and strong gravitational lensing: A brief review, arXiv:1801.00860.
[24] P. V. P. Cunha, C. Herdeiro, E. Radu, and H. F. Runarsson, Shadows of Kerr black holes with scalar hair, Phys. Rev. Lett. **115**, 211102 (2015).
[25] P. V. P. Cunha, C. Herdeiro, E. Radu, and H. F. Runarsson, Shadows of Kerr black holes with and without scalar hair, Int. J. Mod. Phys. D **25**, 1641021 (2016).
[26] F. H. Vincent, E. Gourgoulhon, C. Herdeiro, and E. Radu, Astrophysical imaging of Kerr black holes with scalar hair, Phys. Rev. D **94**, 084045 (2016).
[27] P. V. P. Cunha, J. Grover, C. Herdeiro, E. Radu, H. Runarsson, and A. Wittig, Chaotic lensing around boson stars and Kerr black holes with scalar hair, Phys. Rev. D **94**, 104023 (2016).
[28] J. O. Shipley and S. R. Dolan, Binary black hole shadows, chaotic scattering and the Cantor set, Classical Quantum Gravity **33**, 175001 (2016).
[29] A. Bohn, W. Throwe, F. Hbert, K. Henriksson, and D. Bunandar, What does a binary black hole merger look like?, Classical Quantum Gravity **32**, 065002 (2015).
[30] J. Grover and A. Wittig, Black hole shadows and invariant phase space structures, Phys. Rev. D **96**, 024045 (2017).
[31] P. V. P. Cunha, E. Berti, and C. A. R. Herdeiro, Light ring stability in ultra-compact objects, Phys. Rev. Lett. **119**, 251102 (2017).
[32] P. V. P. Cunha, J. A. Font, C. Herdeiro, E. Radu, N. Sanchis-Gual, and M. Zilhão, Lensing and dynamics of ultra-compact bosonic stars, Phys. Rev. D **96**, 104040 (2017).
[33] R. P. Eatough, H. Falcke, R. Karuppusamy, K. J. Lee, and D. J. Champion, A strong magnetic field around the supermassive black hole at the centre of the Galaxy, Nature (London) **501**, 391 (2013).
[34] J. A. F. Zakharov, N. S. Kardashev, V. N. Lukash, and S. V. Repin, Magnetic fields in AGNs and microquasars, Mon. Not. R. Astron. Soc. **342**, 1325 (2003).
[35] S. A. Tyulbashev, Magnetic fields around AGNs at large and small scales, Astron. Astrophys. **387**, 818 (2002).
[36] R. Turolla, S. Zane, and A. L. Watts, Magnetars: the physics behind observations. A review, Rep. Prog. Phys. **78**, 116901 (2015).
[37] R. D. Blandford and R. L. Znajek, Electromagnetic extraction of energy from Kerr black holes, Mon. Not. R. Astron. Soc. **179**, 433 (1977).
[38] R. D. Blandford and D. G. Payne, Hydromagnetic flows from accretion discs and the production of radio jets, Mon. Not. R. Astron. Soc. **199**, 883 (1982).
[39] B. Punsly, *Black Hole Gravitohydromagnetics*, 2nd ed. (Springer-Verlag, Berlin, 2008).
[40] F. J. Ernst, Black holes in a magnetic universe, J. Math. Phys. (N.Y.) **17**, 54 (1976).
[41] W. B. Bonner, An exact solution of the Einstein-Maxwell equations referring to a magnetic dipole, Z. Phys. **190**, 444 (1966).
[42] O. Kopáček, J. Kovář, V. Karas, and Y. Kojima, Regular and chaotic motion in general relativity: The case of a massive magnetic dipole, in *Relativity and Gravitation 100 Years*

after Einstein in Prague, edited by J. Bičák and T. Ledvinka (Springer, New York, 2014), p. 373.
[43] L. A. Pachón, J. A. Rueda, and J. D. Sanabria-Gómez, Realistic exact solution for the exterior field of a rotating neutron star, Phys. Rev. D **73**, 104038 (2006).
[44] O. G. Andree, B. Javier, C. Iván, and F. Francisco, A visualization of null geodesics for the Bonnor massive dipole, Revista de Matemática: Teoría y Aplicaciones **22**, 255 (2015).
[45] R. Emparan, Black diholes, Phys. Rev. D **61**, 104009 (2000).
[46] H. Fujisaki, Comments on thermal aspects of black diholes, Nuovo Cimento Soc. Ital. Fis. **121B**, 217 (2006); Comments on thermal aspects of the Bonnor-type black dihole in the Brans-Dicke paradigm, Europhys. Lett. **80**, 20004 (2007).
[47] D. M. Zipoy, Topology of some spheroidal metrics, J. Math. Phys. (N.Y.) **7**, 1137 (1966).
[48] B. H. Voorhees, Static axially symmetric gravitational fields, Phys. Rev. D **2**, 2119 (1970).
[49] G. Gomez, J. Llibre, R. Martinez, and C. Simo, *Dynamics and Mission Design Near Libration Points, Volume I: Fundamentals: The Case of Collinear Libration Points* (World Scientific, Singapore, 2001).
[50] G. Mingotti, F. Topputo, and F. Bernelli-Zazzera, Low-energy, low-thrust transfers to the Moon, Celest. Mech. Dyn. Astron. **105**, 61 (2009).
[51] W. S. Koon, M. W. Lo, J. E. Marsden, and S. D. Ross, Low energy transfer to the Moon, Celest. Mech. Dyn. Astron. **81**, 63 (2001).
[52] G. Gómez, W. S. Koon, M. W. Lo, J. E. Marsden, J. Masdemont, and S. D. Ross, Invariant manifolds, the spatial three-body problem and space mission design, Advances in Astronautical Sciences **109**, 1167 (2001).
[53] K. Meyer, G. Hall, and D. Offin, Introduction to Hamiltonian dynamical systems and the *N*-body problem, Applied mathematical sciences **90**, 271 (2009).
[54] M. Wang, S. Chen, and J. Jing (to be published).